

LOW-LIGHT IMAGE ENHANCEMENT VIA WEIGHTED FRACTIONAL-ORDER MODEL

Jun LI, Chao YAN, Qinglu HOU, Weiwei ZHOU

*Quanzhou Institute of Equipment Manufacturing
Chinese Academy of Sciences, Quanzhou, China
e-mail: chaoyan06@163.com*

Yin GAO*

*Fujian Institute of Research on the Structure of Matter
Chinese Academy of Sciences, Fuzhou, China
e-mail: yingao@fjirsm.ac.cn*

Abstract. Low-light image enhancement (LLIE) enables to serve high-level vision tasks and improve their efficiency. Retinex-based methods have well been recognized as a representative technique for LLIE, but they still suffer from inflexible regularization terms in decomposing illumination and reflectance. In this paper, we propose a new weighted fractional-order variational model based on the Retinex model. First, the constructed weighted fractional-order variational model estimates piecewise smoothed and weakly pixel-shifted illumination by aware structures and textures. Then, to solve this problem accurately, we chose a semi-decoupled approach and an alternating minimization method. Finally, the designed multi-illumination fusion method accurately enhances the structure-rich dark regions of the image through well-exposedness and local entropy weights, while realizing adaptive enhancement based on a naturalness-preserving parameter estimation algorithm. The results of subjective and objective experiments on several challenging low-light datasets demonstrate that our proposed method shows better competitiveness in enhancing low-light images compared with the state-of-the-art methods.

Keywords: Low-light image enhancement, fractional-order, adaptive enhancement, Retinex model, multi-illumination fusion

Mathematics Subject Classification 2010: 68-U10

* Corresponding author

1 INTRODUCTION

With the rapid development of imaging technologies and electronics, the environment in which images are captured has become diverse. When the ambient lighting is not ideal, especially in low-light conditions the imaging quality is affected severely, resulting in degraded performance for high-level vision tasks, such as object detection, semantic segmentation, and autonomous driving [1]. Low-light image enhancement techniques are widely employed to improve the contrast and visual quality of captured images, and future computer vision applications will benefit from enhanced images to improve performance. As a result, low-light image enhancement techniques have increasingly become the research focus [2].

Earlier image enhancement methods [3, 4] adjusted the histogram distribution based on the low-light images properties, namely histogram equalization (HE). The goal of HE is to expand the gray-scale distribution of pixels to improve the contrast [5, 6]. These methods take a global perspective leading to over-enhancement and artifacts, and several HE-based methods have been proposed to overcome these shortcomings [7, 8, 9, 10]. However, the HE-based approaches often lead to noise amplification and color distortion.

Aiming to enhance low-light images naturally, Retinex theory [11] provides the physical support for low-light image enhancement with the assumption that the image can be decomposed into illumination and reflectance maps. Typically, single-scale retinex (SSR) [12] and multi-scale retinex (MSR) [13] estimated the illumination by Gaussian filtering, but it is not accurate. To accurately decompose the input image, various integer-order variational models [14, 15, 16, 17, 18, 19] are designed to obtain smooth illumination and structure-rich reflectance, but they either ignore noise or lose image structures. In contrast, the fractional-order variational models [20, 21, 22] have wider range of constraints and can be set with different regularization terms for illumination and reflectance. Since the solution of the Retinex model is a mathematically ill-posed problem, different priors and constraints lead to significantly different results.

With the rapid improvement of computer hardware performance, low-light image enhancement methods based on deep learning have developed rapidly in recent years [23]. Methods represented by supervised learning strategy are LLNet [24], Retinex-Net [25], KinD [26] and DeepUPE [27]. Other methods that do not rely on paired training data include Zero-DCE [28], RUAS [29], EnlightGAN [30] and SCI [31]. There is no denying that these deep networks have powerful fitting performance. However, they are not robust, showing undesirable exposure and color in real-world scenarios.

Inspired by [20, 22, 32], a novel weighted fractional-order variational model is developed for low-light image enhancement. To estimate an accurate illumination map in the L_p norm, the weighted L_p norm is designed for piecewise smoothing by aware local structures. For this nonlinear optimization problem, we use an alternating minimization scheme to find the optimum. To address the shortcoming that Gamma correction loses the structures of local high-intensity regions, the multi-

illumination fusion method uses adaptive parameter estimation to enhance the illumination sequence, and the designed well-exposedness and local entropy weights fusion to obtain illumination with appropriate exposure and contrast. Comparing the state-of-the-art methods, subjective and objective experiments have proved the superior performance of our method. Our main contributions can be summarized as follows:

- The proposed decomposition model iteratively solutions the illumination and reflectance through the weighted fractional-order variational model to obtain piecewise smooth illumination while keeping its pixel intensities consistent with the original image.
- The multi-illumination fusion method achieve adaptive enhancement of illumination sequence by integrating the image brightness distribution and the local entropy that reveal hidden structures, ensuring excellent visibility in both bright and dark regions.
- We validate the advances of the proposed method on six challenging low-light datasets. Subjective assessment, no-reference metrics, and full-reference metrics indicate our method has the competitive performance.

2 RELATED WORK

Various algorithms have been developed to improve the visibility of low-light images, which can be generally classified as histogram equalization, Retinex decomposition and deep learning.

2.1 Histogram Equalization

The methods based on histogram equalization that balance the histogram distribution are the fundamental image enhancement techniques that are computationally efficient and simple to implement [3, 5, 6, 33]. However, the narrow histogram distribution of low-light images often leads to brightness over-saturation and color distortion [34]. To overcome this limitation, several optimization methods have been proposed by scholars in recent years. For instance, Ibrahim et al. [8] developed a method that preserves the mean brightness of the input image inside the output image, resulting in an output image with mean intensity almost equal to that of the input image. Lee et al. [35] proposed a contrast enhancement algorithm that finds differences between two-dimensional histogram layers. Celik and Tjahjadi [36] aimed to remap the histogram by finding a maximum grey-scale difference. Sujee and Padmavathi [9] used histogram matching and the pyramid technique [37] to extract maximum information to achieve enhanced images. Although these methods have simple algorithms and require small computational effort, their enhancement results often suffer from over-enhancement, noise amplification, color deviation, and detail loss [38].

2.2 Retinex Decomposition

Retinex theory [11] is based on the human visual system, which assumes that an image can be decomposed into an illumination map of light variations and a reflectance map that approximates an enhanced image. The early methods processed only the illumination component and then obtained the reflectance component as the enhancement result by element-wise division. SSR [12] and MSR [13] employed Gaussian filtering to obtain the illumination. Xiao and Shi [39] applied a bilateral filter to improve halo artifacts. LIME [14] employed relative total variation (RTV) [40] to solve for illumination, obtaining piecewise smooth illumination that is somewhat representative of the brightness and darkness variations of the input image. It is not rigorous to constrain only illumination in the Retinex decomposition. In order to solve the illumination and reflectance simultaneously, various integer-order regularization constraints [15, 16, 19] are designed to perform piecewise smoothing of illumination and maintain structures on reflectance. Fu et al. [15] proposed a weighted variational model to improve the distortion of the image gradient caused by the logarithmic transform. STAR [19] introduced the exponential mean local variance filter to extract the structures and textures maps. Although they constrain illumination and reflectance, there is no optimization for noise. Considering the noise inherent in low-light images, many optimization methods have been proposed recently. The robust Retinex model (RRM) [17] and semi-decoupled decomposition (SDD) [18] performed the denoising process in the overall image and the reflectance map, respectively. LR3M [41] developed low-rank regularization to denoise particularly well. In contrast to integer-order variational models, fractional-order models produce more flexible constraint effects. The hybrid variational models [20, 22] employed fractional-order norm and L_2 norm for illumination and reflectance respectively, while the fractional-order variational model [21] employs fractional-order norm for both illumination and reflectance. Since the decomposition of the Retinex model is an ill-posed problem, the existing methods need to be more accurate for the decomposition of illumination and reflectance and improperly handle noise.

2.3 Deep Learning

Low-light enhancement methods based on deep learning attract more attention due to the excellent effect in robustness and accuracy. LLNet [24] designed a variant of stacked-sparse noise reduction autoencoder, which can brighten low-light images and reducing noise simultaneously. Lv et al. [42] developed a multi-branch low-light enhancement network based on extracting features at multi-levels to reconstruct images by multi-branch fusion. To improve the performance of the present models, some learning-based methods [25, 26, 43, 44] incorporate the Retinex theory into their network. Wei et al. [25] proposed a Retinex-Net based on deep learning, which includes a Decom-Net that decomposes the input images and an Enhance-Net that adjusts the illumination to improve low-light images. Wu et al. [44] designed a Retinex-based deep unfolding network (URetinex-Net), which cast the optimiza-

tion problem into a learning problem. However, these methods are unsatisfactory under complex conditions due to the usage of paired data. To solve this problem, the unsupervised learning methods without paired data were proposed. Li et al. [45] developed a method called zero-reference deep curve estimation (Zero-DCE++) to adjust the image by estimating curves. This non-reference network has superior performance in optimizing problems of overfitting and generalization. Ma et al. [31] proposed a self-calibrating illumination network (SCI), which utilizes unsupervised training losses to improve the performance of the network. Besides, some GAN-based methods [30, 46] have been successfully applied in the low-light enhancement problem. However, GAN-based models require much more computing time than others. Although the presented learning-based methods have a certain effects to enhance low-light images, their enhancement results commonly suffer from over-exposure, anomalous artifacts and color deviation.

3 PROPOSED METHOD

In this section, a novel weighted fractional-order variational model for low-light image enhancement is proposed based on the Retinex theory. Firstly, the construction of the weighted fractional-order variational model is introduced. Then, an alternating minimization algorithm is employed to obtain the closed solution. Finally, multi-illumination fusion method with improved visual quality maps is constructed to obtain visually effective enhancement results.

3.1 Retinex Model

The traditional Retinex model can be described as:

$$I = L \circ R, \quad (1)$$

where I is the input low-light image. L and R are the illumination and reflectance maps, respectively. The operator \circ denotes the pixel-wise multiplication.

The illumination map represents the brightness variation in different regions of the input image, which we assume to be piecewise smooth. The intrinsic qualities of the observed object are represented by the reflectance map, which is full of textures and structures. A novel weighted fractional-order variational model is employed to estimate the appropriate illumination and reflectance.

3.2 Weighted Fractional-Order Variational Model

Previous variational models [14, 15, 17, 18, 19, 41, 47, 48] adopted the L_1 norm or L_2 norm to regularize the illumination and reflectance, respectively. In contrast, L_p norm ($0 < p < 1$) has better sparse ability to achieve piecewise smoothness [22], which can be performed on the illumination map to obtain more accurate results.

Therefore, the proposed weighted fractional-order variational model can be formulated as an energy minimization problem.

$$\min_{L,R} \|I - L \circ R\|_2^2 + \alpha \|W \circ \nabla L\|_{p_1}^{p_1} + \beta \|\nabla R\|_2^2, \quad (2)$$

where I, L, R are the observed image, illumination map, and reflectance map, respectively. α and β are the balancing parameters for regularizing different terms. $\|\cdot\|_2$ and $\|\cdot\|_p$ represent the L_2 norm and L_p norm, respectively. ∇ is the first-order differential operator, including horizontal ∇_h and vertical ∇_v gradients. W is the weight matrix to highlight the small structures.

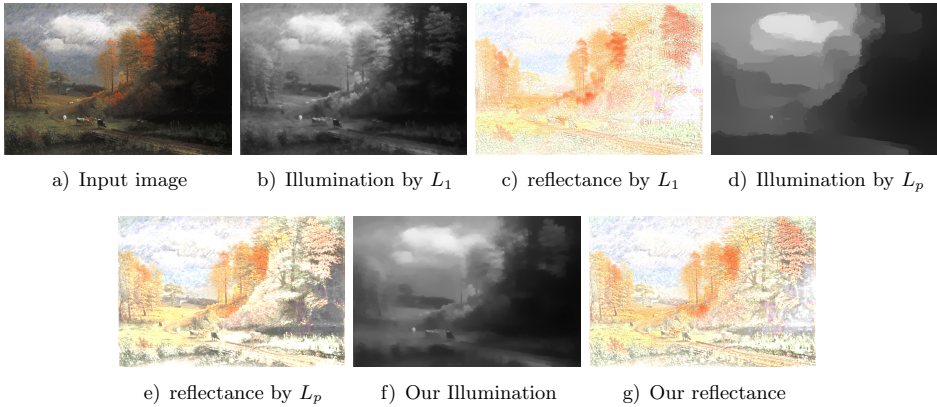


Figure 1. Comparison of illumination and reflectance maps for different norm decomposition with the same smoothing parameters

Most of the existing studies performed integer-order norms on the gradient. LIME [14] proposed the L_1 norm for the relative total variance [40] of illumination. JieP [16] proposed the L_1 norm for the sparsity of the total variation in reflectance and the weighted L_1 norm for the illumination gradient. RRM [17] and LR3M [41] simply adopted the L_1 norm and L_2 norm on the illumination and reflectance gradient, respectively. SDD [18] designed the Gaussian total variation on the L_1 norm to improve the edge-preserving filtering. STAR [19] developed a structure and texture-aware Retinex model for the L_2 norm. HVM [20] and PPRM [22] adopted fractional-order norm to constrain the illumination, and L_2 norm was still used for the reflectance cannot handle single-point noise. Figure 1 shows the illumination and reflectance maps decomposed by the integer-order and fractional-order norms. The smoothing effect of L_1 norm is not significant, and it is not flexible, as shown in Figure 1 b), and it can be seen that our weighted fractional-order variational model performs significantly. In addition, the simple L_p norm produces unnaturally sharp edges in Figure 1 d). In contrast, the proposed weighted fractional-order variational model has a natural and significant smoothing effect.

3.3 Alternative Solution

The solution of Equation (2) is a non-convex problem, we adopt the semi-decoupled method [18] to separate the solution of illumination from reflectance, and then a block coordinate descent algorithm [49] is used to find the optimal solution. Inspired by [20], to efficiently solve the L_p norm, we use an iteratively re-weighted least squares method [50] to rewrite the L_p regularization term as:

$$\|\nabla L\|_{p_l}^{p_l} = (\nabla L + \epsilon)^{p_l-2} \|\nabla L\|_2^2, \quad (3)$$

where ϵ is a small constant. In addition, Equation (2) can be rewritten as

$$\min_{L,R} \|I - L \circ R\|_2^2 + \alpha U_L W \|\nabla L\|_2^2 + \beta \|\nabla R\|_2^2, \quad (4)$$

where $U_L = (\nabla L + \epsilon)^{p_l-2}$. It is worth mentioning that each iteration treats U_L and W as known variables, which are all calculated from the variables of the previous iterations, and then solves the two separate sub-problems sequentially.

To avoid the unknown variable R during the L estimation process, illumination L is obtained utilizing the semi-decoupled approach [18]. Specifically, the illumination L is estimated from the initial illumination map \hat{L} . Similar to [14], \hat{L} is obtained from the maximum of the RGB three channels of the input image.

$$\hat{L}(x) = \max_{c \in \{R,G,B\}} I^c(x). \quad (5)$$

3.3.1 Solution L Sub-Problem

Keeping the terms related to L , we have:

$$\min_L \|L - \hat{L}\|_2^2 + \alpha U_L W \|\nabla L\|_2^2. \quad (6)$$

The illumination solution only involves quadratic terms, differentiating it with respect to L and setting the derivative to zero can be translated into the following problem:

$$(\mathbf{1} + \alpha \sum_{d \in \{h,v\}} \mathbf{M}_d) \mathbf{L} = \hat{\mathbf{L}}, \quad (7)$$

where $\mathbf{1}$ is the identity matrix, $\mathbf{M}_d = \mathbf{D}_d^T \mathbf{U}_L \mathbf{W} \mathbf{D}_d$. In addition, \mathbf{L} , $\hat{\mathbf{L}}$, \mathbf{U}_L , \mathbf{W} are the diagonal matrix representations of L , \hat{L} , U_L , W , respectively. \mathbf{D} contains horizontal \mathbf{D}_h and vertical \mathbf{D}_v , which are the Toeplitz matrices from the discrete gradient operators with a forward difference.

3.3.2 Solution R Sub-Problem

By removing the term unrelated to R , we have the target function:

$$\min_R \|I - L \circ R\|_2^2 + \beta \|\nabla R\|_2^2. \quad (8)$$

Using a similar procedure to solve L , we have the following equation:

$$(\mathbf{L}^2 + \beta \sum_{d \in \{h, v\}} \mathbf{D}_d^T \mathbf{D}_d) \mathbf{R} = \mathbf{L}^T \mathbf{I}. \quad (9)$$

The updates stop when the convergence condition $\|R^{(k+1)} - R^{(k)}\|_F / \|R^{(k)}\|_F < \epsilon$ or $\|L^{(k+1)} - L^{(k)}\|_F / \|L^{(k)}\|_F < \epsilon$ is satisfied, or until the maximum number of iterations K . To improve computational efficiency, a fast solver called preconditioned conjugate gradient (PCG) [51] is used for speed up. In Figure 10, appropriate illumination and reflectance can be obtained through 10 iterations. Further, the parameters are set and fixed to $\epsilon = 10^{-2}$ and $K = 10$.

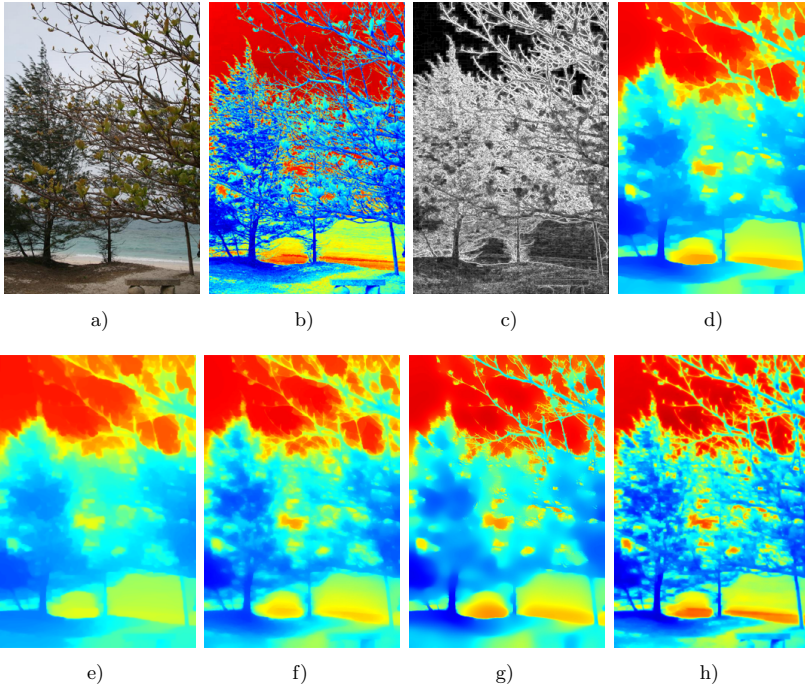


Figure 2. Comparison of estimated illumination with (w/) and without (w/o) weighting matrix W . a) Input. b) Initial illumination map \hat{L} . c) Weight W for illumination. d) Illumination w/o W . e) Illumination of LIME [14]. f) Illumination of SDD [18]. g) Illumination of PPRM [22]. h) Our illumination.

3.4 Weight Matrix for Illumination

The major edges can be preserved by L_p norm regulating illumination, but the smoothness of the internal structures still needs improvement [22]. As demonstrated

in Figure 2h), the weighted fractional-order variational model maintains fine structures and small overall pixel offsets, which means that the estimated illumination is more accurate.

The matrix of weights W is designed to adjust the smoothness of various regions. To prevent the development of redundant structures, W detects the regional features and improves minor structures. Each pixel in W is computed using two components, $W_A(x)$ and $\|\nabla L(x)\|_2$.

$$W(x) = \sqrt{(W_A(x) \circ \|\nabla L(x)\|_2)}. \tag{10}$$

For each pixel x in L , $W_A(x)$ is based on the magnified illumination gradient. In order to be aware of surrounding neighborhoods and decrease noise effects, the Gaussian filter G_σ with kernel size σ when calculating:

$$W_A(x) = e^{1-|\nabla(G_\sigma * L)|}. \tag{11}$$

Furthermore, $W_A(x)$ is particularly sensitive to fine textures and structures. $\|\nabla L(x)\|_2$ can roughly identify the shapes and scopes of different objects. $W(x)$ combines two weights to maximize the utility of both terms.

Figure 2 shows the illumination obtained from different decomposition methods, LIME cannot maintain the small structures between branches and the pixels are heavily shifted. Without weights W and SDD show local connectivity when dealing with branched structures, and PPRM fails to maintain some of the small structures within the object. For contrast, the proposed weighted fractional-order variational model efficiently preserves various small structures while the pixel intensities are highly consistent with the input image, indicating that the estimated illumination is more accurate.

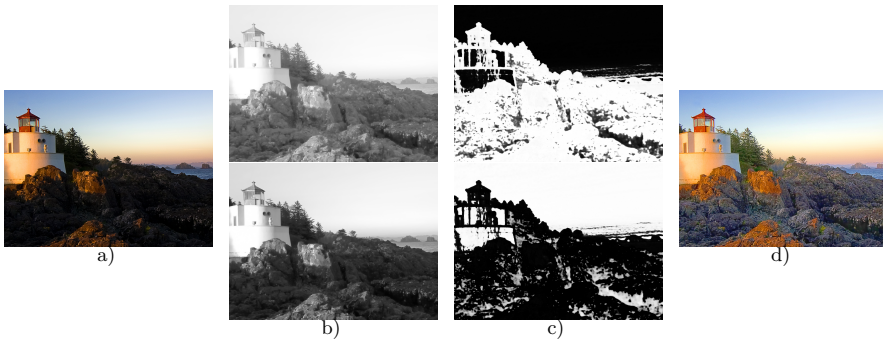


Figure 3. Example of the proposed multi-illumination fusion method. a) Input image. b) Illumination sequence obtained with two different Gamma corrections. c) Fusion weight maps corresponding to illumination sequence. d) Enhanced image.

3.5 Multi-Illumination Fusion

The illumination map obtained from the decomposition is performed Gamma correction and combined with the reflectance map to obtain the enhancement image [14, 17, 18, 19, 20, 22, 41]. We propose a new multi-illumination fusion method that performs fusion of illumination sequence obtained from different Gamma corrections, which is capable of producing high-quality enhancement results.

Figure 3 illustrates the specific flow of the proposed multi-illumination fusion method. For the estimated original illumination L , two different Gamma corrections are performed to obtain the enhanced illuminations ($L_g^k = L^{\lambda_k}, k = \{1, 2\}$). λ_1 and λ_2 perform different levels of enhancement of the illumination L to obtain a wider range of image brightness. Assuming $\lambda_1 + \lambda_2 = 1$ ($\lambda_1 < \lambda_2$), it can be known that illumination L_1 serves to enhance the dark regions of the image, while L_2 maintains the local high-intensity regions in the image. Therefore, the enhanced image is represented as:

$$\hat{I} = h(L, R, \lambda) = R \circ \sum_{k=1}^2 \hat{\mathcal{W}}_p^k L_{g,p}^k, \quad (12)$$

where $h(L, R, \lambda)$ denotes the final illumination obtained by performing two Gamma corrections ($\lambda_1 = \lambda, \lambda_2 = 1 - \lambda$) on the estimated illumination and fusing them, which is then combined with the reflectance to calculate the enhanced result \hat{I} . $\hat{\mathcal{W}}_p^k$ represents the fusion weights corresponding to the illumination sequence $\{L_g^1, L_g^2\}$, as shown in Figure 3c). The traditional exposure fusion algorithm [32] contains three fusion weights of contrast, saturation and well-exposedness. In order to better enhance the dark regions structures of the input image, we use two features of well-exposedness and local entropy for fusion, which can be expressed as:

$$\mathcal{W}_p^k = (E_p^k)^{\gamma_e} \times (T_p^k)^{\gamma_t}, k \in \{1, 2\}, \quad (13)$$

where k indicates the k^{th} image in the illumination sequence. p represents a pixel in the image. E and T are quantitatively measures for well-exposedness and local entropy. γ_e and γ_t are parameters for controlling the influence of each measure, which are set to 1 by default. Note, pixels with higher visual quality values are more likely better exposed.

Figure 4 demonstrates the well-exposedness and local entropy weights corresponding to the illumination sequence and the computation process, and it can be seen that the proposed method prefers regions with good visual sense. As shown in Figure 5c), the visualization of the exposure fusion [32] results is unsatisfactory, and it does not give enough exposure to the dark regions of the image. In order to blend the illumination more rationally, in this paper, the well-exposedness weights are constructed as follows:

$$E_p^k = \exp\left(\frac{-10(L_{g,p}^k - 0.6)^2}{\sigma}\right), \quad (14)$$

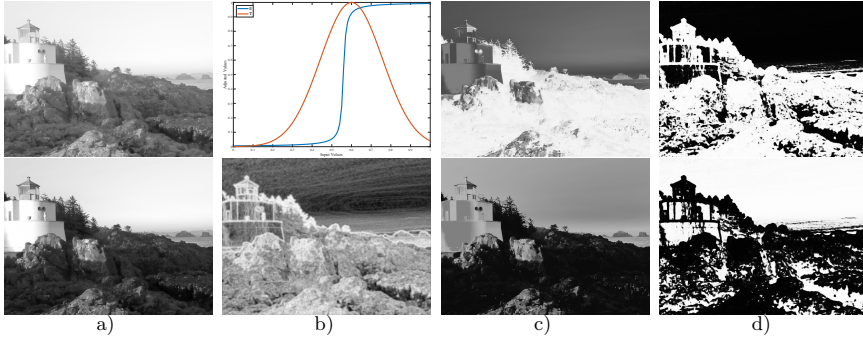


Figure 4. The proposed multi-illumination fusion method of the well-exposedness and local entropy weights. a) Illumination sequence $\{L_g^1, L_g^2\}$. b) First row: curves of Equation (14) and (15), Second row: normalized local entropy $\mathcal{N}(\mathcal{E})$. c) Well-exposedness wights $\{E_p^1, E_p^2\}$. d) Local entropy weights $\{T_p^1, T_p^2\}$.



Figure 5. Comparison of enhancement results obtained by different fusion methods on illumination sequence. a) Input image. b) Gamma Correction. c) Exposure Fusion [32]. d) Ours.

where $L_{g,p}^k$ represents the pixel p of the k^{th} image in the $\{L_g^1, L_g^2\}$.

For more rational fusion of illumination sequence, the regions with high local entropy values and darkness in the input image should have a greater weight on L_1 , while the high-intensity regions of the image itself should have a greater weight on L_2 , and the weight T_p^k of the illumination sequence is constructed as respectively:

$$T_p^1 = \frac{1}{\pi} \arctan \left(100 \left(\mathcal{N}(\mathcal{E}) - \frac{3.5}{\max(\mathcal{E})} \right) \right), T_p^2 = 1 - T_p^1, \quad (15)$$

where \mathcal{E} represents the local entropy of the input image and \mathcal{N} is the operator that normalizes it to $[0, 1]$. The local entropy is highly robust to low-light images as shown in Figure 4 b). The calculation of local entropy can be obtained by having

the following equation:

$$\mathcal{E}(x) = -\frac{1}{N} \sum_{y \in \Omega(x)} I_g \ln(I_g(y)), \quad (16)$$

where I_g represents the gray image of the input image. $\Omega(x)$ is a local patch centered at x , and N is the number of pixels in the patch. To obtain a consistent result, the two visual quality mappings corresponding to the sequence $\{L_g^1, L_g^2\}$ are then normalized so that they sum to 1 at each pixel p :

$$\hat{\mathcal{W}}_p^k = \left[\sum_{i=1}^2 \mathcal{W}_p^i \right]^{-1} \mathcal{W}_p^k. \quad (17)$$

Algorithm 1 LLIE via Weighted Fractional-Order Model

Input: The low-light image I .

Initialization: $\alpha = 2\text{mean}(|\nabla I|)$, $\omega = 0.001$, $p_l = 0.9$, $K = 10$.

for $k = 0$ to K **do**

Update $L^{(k+1)}$ via Equation (7);

Update $R^{(k+1)}$ via Equation (9);

if converged **then**

break;

end if

end for

Estimate $\hat{\lambda}$ via Equation (18);

Estimate $\hat{\mathcal{W}}$ via Equation (17);

Estimate \hat{I} via Equation (12);

Output: The estimated result \hat{I} .

It is a challenge to reasonably compute the parameter λ in Equation (12), for which we design an optimization function. By making the enhancement results have better naturalness, we minimize its NIQE metrics to estimate a suitable parameter:

$$\hat{\lambda} = \min_{\lambda} \mathcal{Q}(h(L, R, \lambda)), \quad (18)$$

where \mathcal{Q} represents the operator that computes the image NIQE [52] metrics, and The optimized λ can be solved by one-dimensional minimizer.

Figure 5 d) shows the enhancement results obtained from the improved visual quality maps, where we obtain sharper images with better contrast and color. Given an input low-light image, the whole process of our method to enhance the image is summarized in Algorithm 1.

4 EXPERIMENTS

In this section, we compare the proposed method to state-of-the-art methods in both subjective and objective assessments. For fair comparisons, we fix the parameters $\{\alpha = 2\text{mean}(|\nabla I|), \beta = 0.001, p_l = 0.9\}$ in all tests. Furthermore, all comparison methods are generated on the authors' websites and use the default settings. We run the experiments in MATLAB R2022a and PyCharm 2022 on a PC with Windows 10 OS.

4.1 Experiment Settings

We compare the proposed approach with several state-of-the-art methods, including LIME [14], RRM [17], SDD [18], PCA [53], Zero-DCE++ [45], SCI [31], PPRM [22], URetinex-Net [44] and PairLIE [54]. The test images are obtained from five public datasets: DICM [35], Fusion [55], LIME [14], MEF [56], NPE [57]. The second test dataset is SICE [58] with more than 100 images and ground truth, where we resized the images to 25% of their original size owing to the memory usage limitations of the different methods. Each test image is taken in RGB format and contains a variety of dimensions and scenes.

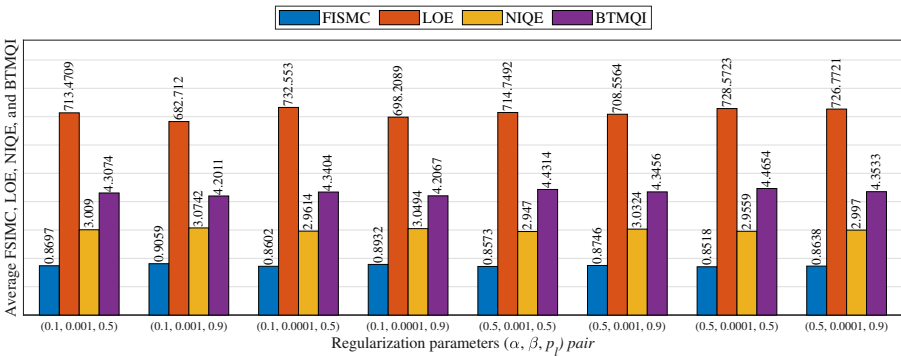


Figure 6. Average FSIMC, LOE, NIQE, and NTMQI results on six public datasets using the proposed method with different regularization parameters

4.2 Parameters Study

In this section, we evaluate the role of the regularization parameters α, β, p_l for Equation (2). The objective results for different (α, β, p_l) pairs on all test images are given in Figure 6, where the range of α belongs to $\{0.1, 0.5\}$, β is chosen from $\{0.001, 0.0001\}$, and the values of p_l are set to $\{0.5, 0.9\}$, respectively. It can be seen that $(0.1, 0.001, 0.5)$, $(0.1, 0.001, 0.9)$ and $(0.1, 0.0001, 0.9)$ have higher FSIMC

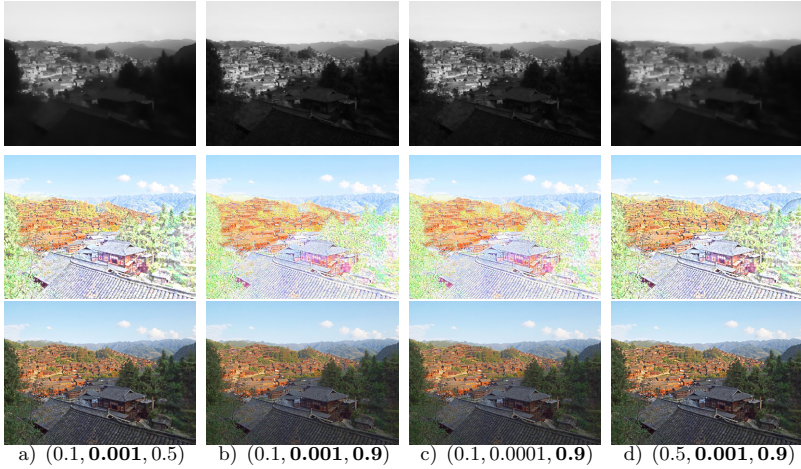


Figure 7. Examples of impact of (α, β, p_l) pairs. First row: estimated illumination maps. Second row: estimated reflectance maps. Third row: enhanced images. Default settings are highlighted in bold.

and also lower values in LOE, NIQE and BTMQUI, where $(0.1, 0.001, 0.9)$ has highest FSIMC and lowest LOE.

Figure 7 further demonstrates the effect of different α, β, p_l on the illumination, reflectance and enhanced results. It can be observed that α affects the overall smoothness of the illumination, with the larger it is the smoother the illumination is. The parameter β serves to balance the noise and textures in the reflectance map. For parameter p_l , it describes the ability of the illumination map to smooth the textures. Different images contain different degrees of textures and structures, and in order to adaptively obtain smooth illumination, in our experiments, α is set to correlate with the mean value of the image gradient, and the parameters are set to $\{\alpha = 2\text{mean}(|\nabla I|), \beta = 0.001, p_l = 0.9\}$ for all test images.

4.3 Subjective Assessments

We compare the visual effects of the proposed method with the state-of-the-art methods on different low-light images. The visual results of two common test images are shown in Figures 8 and 9.

In Figure 8, The over-enhancement of LIME and URetinex-Net is impressive and incompatible with human visual senses. SDD, PCA and PPRM have abnormal contrast levels and show unnatural transition at the image edges. All three deep learning methods, Zero-DCE++, SCI and URetinex-Net, suffer from color deflection, possibly due to poor generalization caused by the training dataset. As can be seen in the sky regions, LIME and PPRM seriously amplify the noise, while massive

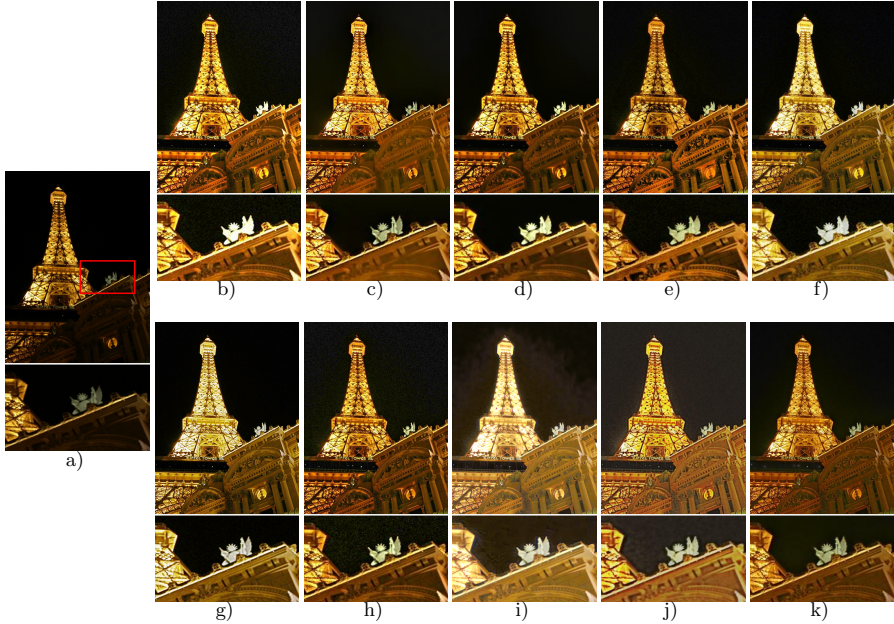


Figure 8. Comparison of enhanced results with state-of-the-art low-light image enhancement methods. a) Input. b) LIME [14]. c) RRM [17]. d) SDD [18]. e) PCA [53]. f) Zero-DCE++ [45]. g) SCI [31]. h) PPRM [22]. i) URetinex-Net [44]. j) PairLIE [54]. k) Ours.

halo artifacts are present in URetinex-Net. PairLIE enhances dark regions, but there are distortion artifacts at the edges and poor denoising. Although RRM denoising is effective, it is accompanied by loss of image structures. Comparatively, the proposed method successfully enhances the dark regions and preserves more textures and details.

Figure 9 demonstrates the experimental results of a non-uniform brightness image. The enlarged regions in Figures 9b), 9d), 9e), 9h) illustrate that there are local regions of over-enhancement in LIME, SDD, PCA, and PPRM, which are undesired results. For clouds in the sky, LIME, RRM, SCI and URetinex-Net can not maintain their structures, reducing images' visibility. Similar to the results in Figure 8, the Zero-DCE++ and SCI have a different tone than the input images and the PCA suffers from a lot of black distortion. PairLIE will over-enhance the entire image while resulting in significant texture loss and a poor overall visual sense. In summary, the proposed method realizes visually clear outcomes while naturally enhancing illumination. Furthermore, our method prevents over-enhancement and color loss in bright regions.

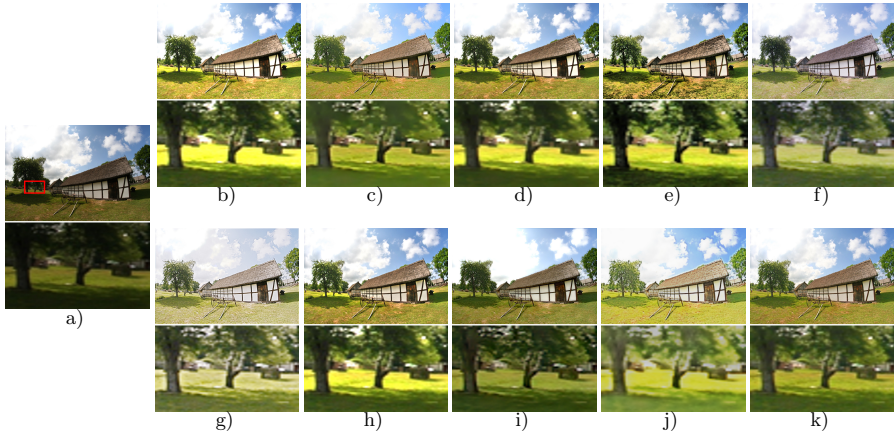


Figure 9. Comparison of enhanced results with state-of-the-art low-light image enhancement methods. a) Input. b) LIME [14]. c) RRM [17]. d) SDD [18]. e) PCA [53]. f) Zero-DCE++ [45]. g) SCI [31]. h) PPRM [22]. i) URetinex-Net [44]. j) PairLIE [54]. k) Ours.

Methods	FSIMC \uparrow	LOE \downarrow	NIQE \downarrow	BTMQI \downarrow
LIME	0.7468	856.4784	3.7092	4.6911
RRM	<u>0.8871</u>	<u>720.4061</u>	3.8528	4.5795
SDD	0.8649	731.1883	3.4460	4.4939
PCA	0.7128	833.5304	3.6685	4.5613
Zero-DCE++	0.8368	782.8061	<u>3.3587</u>	4.4066
SCI	0.7988	778.5065	4.0943	4.9942
PPRM	0.8042	792.9424	3.4434	<u>4.4601</u>
URetinex-Net	0.8261	775.7184	3.6065	4.5512
PairLIE	0.7687	831.0264	3.9192	4.5883
Ours	0.9015	666.5242	3.1799	4.4983

Table 1. Average FSIMC, LOE, NIQE and BTMQI results on the DICM [35], Fusion [55], LIME [14], MEF [56] and NPE [57] datasets

4.4 Objective Assessments

To objectively evaluate the quality of the enhanced images, we use four representative image quality assessments (IQAs), including the feature similarity index for color images [59], lightness order error (LOE) [57], naturalness image quality evaluator (NIQE) [52] and blind tone-mapped quality index (BTMQI) [60]. In general, higher FSIMC values indicate better quality of image structures, smaller LOE values suggest less distortion between the enhanced and input images, lower NIQE values correspond to better image naturalness, and lower BTMQI values indicate better image quality.

Table 1 shows the specific data of the four assessment metrics on the five datasets. The two best performances are marked in bold and underlined. RRM has the second best FSIMC and LOE which indicates that it has less distortion in the enhanced image. The second best NIQE and BTMQUI performance is Zero-DCE++ indicating that it has natural enhancement results. LIME and PCA perform badly in every aspect, proving that the enhancement results have obvious distortion and are not natural. The four metrics of SDD are mediocre, and the enhancement effect can be improved. SCI, PPRM, and URetinex-Net perform unfavorably in most metrics due to the whitish tones of SCI, the amplified noise of PPRM, and the over-enhanced loss of information in URetinex-Net. It can be seen that our approach achieves the best on all four metrics. Comprehensively, the proposed method outperforms other methods in terms of image sharpness, contrast and structural information.

Methods	PSNR	SSIM	FSIMC	LOE	NIQE	BTMQUI
LIME	12.1340	0.4578	0.8024	731.1822	3.1490	5.0484
RRM	14.3789	0.4863	<u>0.9062</u>	710.8631	3.8578	4.1648
SDD	<u>14.5236</u>	<u>0.4875</u>	0.8690	<u>703.8549</u>	3.0494	<u>4.1571</u>
PCA	12.4634	0.4276	0.7712	729.9708	3.3623	4.9304
Zero-DCE++	13.5381	0.3293	0.8700	723.6404	2.6244	4.2356
SCI	14.3624	0.4717	0.8282	728.9347	3.4398	5.0696
PPRM	11.5182	0.3075	0.8410	729.1265	2.8201	4.3987
URetinex-Net	13.3061	0.4192	0.8930	706.8212	3.0343	4.3165
PairLIE	11.7466	0.4147	0.8112	730.2447	3.7213	4.9394
Ours	15.3568	0.4892	0.9125	695.9043	<u>2.6776</u>	3.7950

Table 2. Average PSNR, SSIM, FSIMC, LOE, NIQE and BTMQUI results on the SICE [58] dataset

The PSNR and SSIM metrics are additionally added to the SICE dataset, and all the results are shown in Table 2. The overall metrics of LIME, PCA, PPRM, and PairLIE perform poorly due to the noise effects that usually accompany the enhancement process and the presence of over-enhancement and aberration artifacts. SCI, RRM, URetinex-Net, and Zero-DCE++ similarly perform poorly on few metrics, indicating that they are less robust and cannot take into account the complex scene and noise distributions of low-light images. SDD obtains the second on four metrics, proving its effectiveness in enhancing low-light images but still suffers from structural loss in the denoising process. Comparatively, the proposed method possesses the best results on five metrics, benefiting from the adaptive parameter estimation, which is consistent with our subjective results. The experimental results demonstrate the effectiveness of the designed weighted fractional-order variational model for low-light image enhancement.

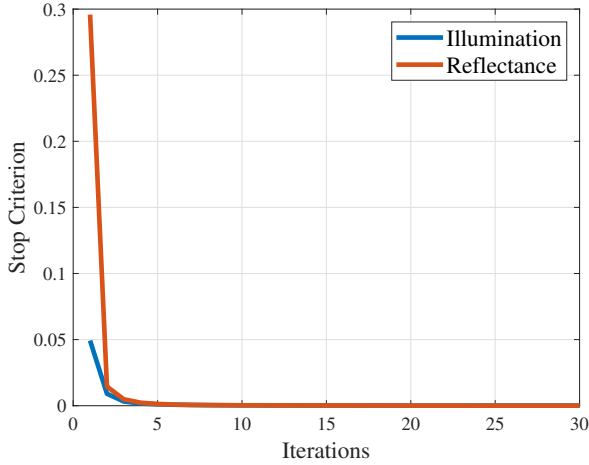


Figure 10. Convergence curve of our model

4.5 Convergence Speed

For the convergence speed of the proposed model, we test it on more than 300 low-light test images, and the average convergence curves of illumination and reflectance are shown in Figure 10. As the number of iterations increases, the curves of illumination and reflectance decrease rapidly and then tend to smooth. The average convergence curves on more than 300 test images show that the proposed method converges significantly faster and within 10 iterations.

For an image of size $480 \times 640 \times 3$, the computational time for all the compared methods are listed as follows: LIME 0.16 s, RRM 22.37 s, SDD 3.96 s, PCA 0.21 s, SCI 0.48 s, PPRM 6.59 s, and Ours 3.72 s. The proposed method is faster than most variational models and our results are the best in both subjective and objective assessments.

4.6 Ablation Study

To evaluate the effectiveness of the proposed weighted fractional-order variational model and the multi-illumination fusion method, Figure 11 shows the importance of the two modules. For the input low-light image, Figure 11 b) shows the output image obtained without using the weighted matrix, which enhances the image brightness but the contrast is not well recovered. Figure 11 c) shows the output image obtained without multi-illumination fusion (using normal Gamma correction enhancement), it can be seen that some regions are low brightness and do not show the structures of the image completely. Figure 11 d) shows the enhancement result obtained by the proposed method, which has excellent brightness and contrast, high visibility and is closest to the ground truth.

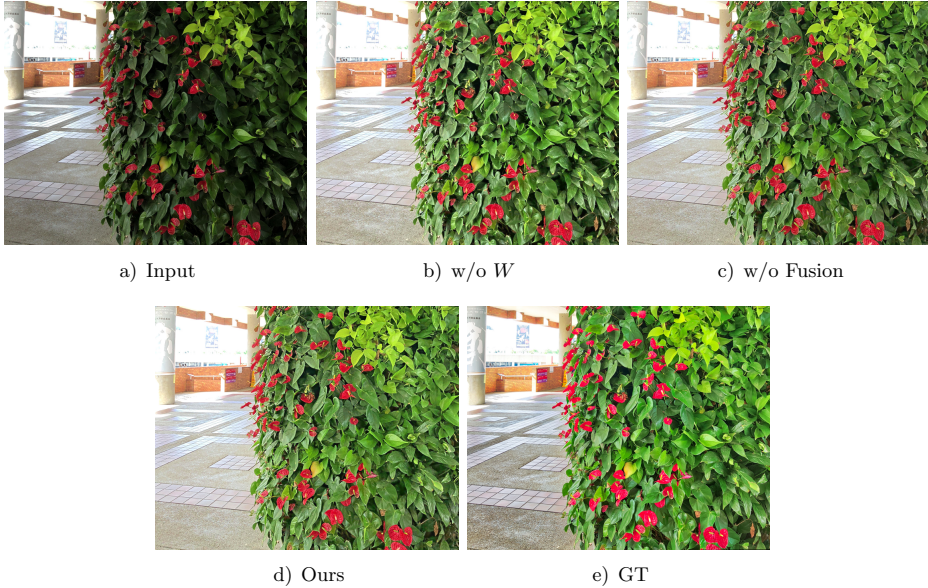


Figure 11. Ablation studies on the framework. 'w/o W ' denotes our method without weighted matrix W introduced in Section 3.4. 'w/o Fusion' denotes our method without multi-illumination fusion method and uses Gamma correction of value 1/2.2 for enhancement. We can observe that our framework is important for low-light enhancement.

5 CONCLUSION

This paper introduces a novel weighted fractional-order variational model for low-light image enhancement. Compared with the current Retinex-based methods, the proposed model can precisely decompose the illumination and reflectance maps. The decomposition model smooths the illumination component while avoiding the loss of local brightness features by aware image's primary structures. The constructed multi-illumination fusion method employs well-exposedness and local entropy weights so that information-rich dark regions are adequately enhanced and the brightness level of localized high-intensity regions is maintained. Subjective and objective evaluation experiments on over 300 challenging low-light images are conducted respectively, and the results demonstrate that the proposed method outperforms the state-of-the-art methods. We believe that this work lays a solid foundation for future enhancement research, and we plan to extend our approach to video enhancement.

Acknowledgment

This work was supported by the National Natural Science Foundation of China (No. 62001452), Fujian Science and Technology Innovation Laboratory for Optoelectronic Information of China (No. 2021ZZ116), Science and Technology Program of Fujian (No. 2020T3027), Science and Technology Program of Fuzhou (No. 2022ZD-001) and Fujian Intelligent Control Technology and Economic Integration Service Platform.

REFERENCES

- [1] XU, K.—CHEN, H.—XU, C.—JIN, Y.—ZHU, C.: Structure-Texture Aware Network for Low-Light Image Enhancement. *IEEE Transactions on Circuits and Systems for Video Technology*, Vol. 32, 2022, No. 8, pp. 4983–4996, doi: 10.1109/TCSVT.2022.3141578.
- [2] YANG, B.—PAN, D.—JIANG, Z.—HUANG, J.—GUI, W.: CSDM: A Cross-Scale Decomposition Method for Low-Light Image Enhancement. *Signal Processing*, Vol. 202, 2023, Art.No. 108752, doi: 10.1016/j.sigpro.2022.108752.
- [3] PIZER, S. M.—AMBURN, E. P.—AUSTIN, J. D.—CROMARTIE, R.—GESELOWITZ, A.—GREER, T.—TER HAAR ROMENY, B.—ZIMMERMAN, J. B.—ZUIDERVELD, K.: Adaptive Histogram Equalization and Its Variations. *Computer Vision, Graphics, and Image Processing*, Vol. 39, 1987, No. 3, pp. 355–368, doi: 10.1016/S0734-189X(87)80186-X.
- [4] PIZER, S. M.—JOHNSTON, R. E.—ERIKSEN, J. P.—YANKASKAS, B. C.—MULLER, K. E.: Contrast-Limited Adaptive Histogram Equalization: Speed and Effectiveness. *Proceedings of the First Conference on Visualization in Biomedical Computing*, 1990, pp. 337–345, doi: 10.1109/VBC.1990.109340.
- [5] STARK, J. A.: Adaptive Image Contrast Enhancement Using Generalizations of Histogram Equalization. *IEEE Transactions on Image Processing*, Vol. 9, 2000, No. 5, pp. 889–896, doi: 10.1109/83.841534.
- [6] CHENG, H. D.—SHI, X. J.: A Simple and Effective Histogram Equalization Approach to Image Enhancement. *Digital Signal Processing*, Vol. 14, 2004, No. 2, pp. 158–170, doi: 10.1016/j.dsp.2003.07.002.
- [7] WANG, C.—YE, Z.: Brightness Preserving Histogram Equalization with Maximum Entropy: A Variational Perspective. *IEEE Transactions on Consumer Electronics*, Vol. 51, 2005, No. 4, pp. 1326–1334, doi: 10.1109/TCE.2005.1561863.
- [8] IBRAHIM, H.—PIK KONG, N. S.: Brightness Preserving Dynamic Histogram Equalization for Image Contrast Enhancement. *IEEE Transactions on Consumer Electronics*, Vol. 53, 2007, No. 4, pp. 1752–1758, doi: 10.1109/TCE.2007.4429280.
- [9] SUJEE, R.—PADMAVATHI, S.: Image Enhancement Through Pyramid Histogram Matching. *2017 International Conference on Computer Communication and Informatics (ICCCI)*, 2017, pp. 1–5, doi: 10.1109/ICCCI.2017.8117748.

- [10] JUNG, C.—SUN, T.: Optimized Perceptual Tone Mapping for Contrast Enhancement of Images. *IEEE Transactions on Circuits and Systems for Video Technology*, Vol. 27, 2017, No. 6, pp. 1161–1170, doi: 10.1109/TCSVT.2016.2527339.
- [11] LAND, E. H.—McCANN, J. J.: Lightness and Retinex Theory. *Journal of the Optical Society of America*, Vol. 61, 1971, No. 1, pp. 1–11, doi: 10.1364/JOSA.61.000001.
- [12] JOBSON, D. J.—RAHMAN, Z.—WOODELL, G. A.: Properties and Performance of a Center/Surround Retinex. *IEEE Transactions on Image Processing*, Vol. 6, 1997, No. 3, pp. 451–462, doi: 10.1109/83.557356.
- [13] JOBSON, D. J.—RAHMAN, Z.—WOODELL, G. A.: A Multiscale Retinex for Bridging the Gap Between Color Images and the Human Observation of Scenes. *IEEE Transactions on Image Processing*, Vol. 6, 1997, No. 7, pp. 965–976, doi: 10.1109/83.597272.
- [14] GUO, X.—LI, Y.—LING, H.: LIME: Low-Light Image Enhancement via Illumination Map Estimation. *IEEE Transactions on Image Processing*, Vol. 26, 2017, No. 2, pp. 982–993, doi: 10.1109/TIP.2016.2639450.
- [15] FU, X.—ZENG, D.—HUANG, Y.—ZHANG, X. P.—DING, X.: A Weighted Variational Model for Simultaneous Reflectance and Illumination Estimation. 2016 IEEE Conference on Computer Vision and Pattern Recognition (CVPR), 2016, pp. 2782–2790, doi: 10.1109/CVPR.2016.304.
- [16] CAI, B.—XU, X.—GUO, K.—JIA, K.—HU, B.—TAO, D.: A Joint Intrinsic-Extrinsic Prior Model for Retinex. 2017 IEEE International Conference on Computer Vision (ICCV), 2017, pp. 4020–4029, doi: 10.1109/ICCV.2017.431.
- [17] LI, M.—LIU, J.—YANG, W.—SUN, X.—GUO, Z.: Structure-Revealing Low-Light Image Enhancement via Robust Retinex Model. *IEEE Transactions on Image Processing*, Vol. 27, 2018, No. 6, pp. 2828–2841, doi: 10.1109/TIP.2018.2810539.
- [18] HAO, S.—HAN, X.—GUO, Y.—XU, X.—WANG, M.: Low-Light Image Enhancement with Semi-Decoupled Decomposition. *IEEE Transactions on Multimedia*, Vol. 22, 2020, No. 12, pp. 3025–3038, doi: 10.1109/TMM.2020.2969790.
- [19] XU, J.—HOU, Y.—REN, D.—LIU, L.—ZHU, F.—YU, M.—WANG, H.—SHAO, L.: STAR: A Structure and Texture Aware Retinex Model. *IEEE Transactions on Image Processing*, Vol. 29, 2020, pp. 5022–5037, doi: 10.1109/TIP.2020.2974060.
- [20] FU, G.—DUAN, L.—XIAO, C.: A Hybrid L2-LP Variational Model for Single Low-Light Image Enhancement with Bright Channel Prior. 2019 IEEE International Conference on Image Processing (ICIP), 2019, pp. 1925–1929, doi: 10.1109/ICIP.2019.8803197.
- [21] GU, Z.—LI, F.—FANG, F.—ZHANG, G.: A Novel Retinex-Based Fractional-Order Variational Model for Images with Severely Low Light. *IEEE Transactions on Image Processing*, Vol. 29, 2020, pp. 3239–3253, doi: 10.1109/TIP.2019.2958144.
- [22] LIN, Y. H.—LU, Y. C.: Low-Light Enhancement Using a Plug-and-Play Retinex Model with Shrinkage Mapping for Illumination Estimation. *IEEE Transactions on Image Processing*, Vol. 31, 2022, pp. 4897–4908, doi: 10.1109/TIP.2022.3189805.
- [23] LI, C.—GUO, C.—HAN, L.—JIANG, J.—CHENG, M. M.—GU, J.—LOY, C. C.: Low-Light Image and Video Enhancement Using Deep Learning: A Survey. *IEEE Transactions on Pattern Analysis and Machine Intelligence*, Vol. 44, 2022, No. 12, pp. 9396–9416, doi: 10.1109/TPAMI.2021.3126387.

- [24] LORE, K. G.—AKINTAYO, A.—SARKAR, S.: LLNet: A Deep Autoencoder Approach to Natural Low-Light Image Enhancement. *Pattern Recognition*, Vol. 61, 2017, pp. 650–662, doi: 10.1016/j.patcog.2016.06.008.
- [25] WEI, C.—WANG, W.—YANG, W.—LIU, J.: Deep Retinex Decomposition for Low-Light Enhancement. *CoRR*, 2018, doi: 10.48550/arXiv.1808.04560.
- [26] ZHANG, Y.—ZHANG, J.—GUO, X.: Kindling the Darkness: A Practical Low-Light Image Enhancer. *Proceedings of the 27th ACM International Conference on Multimedia (MM'19)*, 2019, pp. 1632–1640, doi: 10.1145/3343031.3350926.
- [27] WANG, R.—ZHANG, Q.—FU, C. W.—SHEN, X.—ZHENG, W. S.—JIA, J.: Underexposed Photo Enhancement Using Deep Illumination Estimation. *2019 IEEE/CVF Conference on Computer Vision and Pattern Recognition (CVPR)*, 2019, pp. 6842–6850, doi: 10.1109/CVPR.2019.00701.
- [28] GUO, C.—LI, C.—GUO, J.—LOY, C. C.—HOU, J.—KWONG, S.—CONG, R.: Zero-Reference Deep Curve Estimation for Low-Light Image Enhancement. *2020 IEEE/CVF Conference on Computer Vision and Pattern Recognition (CVPR)*, 2020, pp. 1777–1786, doi: 10.1109/CVPR42600.2020.00185.
- [29] LIU, R.—MA, L.—ZHANG, J.—FAN, X.—LUO, Z.: Retinex-Inspired Unrolling with Cooperative Prior Architecture Search for Low-Light Image Enhancement. *2021 IEEE/CVF Conference on Computer Vision and Pattern Recognition (CVPR)*, 2021, pp. 10556–10565, doi: 10.1109/CVPR46437.2021.01042.
- [30] JIANG, Y.—GONG, X.—LIU, D.—CHENG, Y.—FANG, C.—SHEN, X.—YANG, J.—ZHOU, P.—WANG, Z.: EnlightenGAN: Deep Light Enhancement Without Paired Supervision. *IEEE Transactions on Image Processing*, Vol. 30, 2021, pp. 2340–2349, doi: 10.1109/TIP.2021.3051462.
- [31] MA, L.—MA, T.—LIU, R.—FAN, X.—LUO, Z.: Toward Fast, Flexible, and Robust Low-Light Image Enhancement. *2022 IEEE/CVF Conference on Computer Vision and Pattern Recognition (CVPR)*, 2022, pp. 5627–5636, doi: 10.1109/CVPR52688.2022.00555.
- [32] MERTENS, T.—KAUTZ, J.—VAN REETH, F.: Exposure Fusion: A Simple and Practical Alternative to High Dynamic Range Photography. *Computer Graphics Forum*, Vol. 28, 2009, No. 1, pp. 161–171, doi: 10.1111/j.1467-8659.2008.01171.x.
- [33] ABDULLAH-AL-WADUD, M.—KABIR, M. H.—AKBER DEWAN, M. A.—CHAE, O.: A Dynamic Histogram Equalization for Image Contrast Enhancement. *IEEE Transactions on Consumer Electronics*, Vol. 53, 2007, No. 2, pp. 593–600, doi: 10.1109/TCE.2007.381734.
- [34] XU, Y.—YANG, C.—SUN, B.—YAN, X.—CHEN, M.: A Novel Multi-Scale Fusion Framework for Detail-Preserving Low-Light Image Enhancement. *Information Sciences*, Vol. 548, 2021, pp. 378–397, doi: 10.1016/j.ins.2020.09.066.
- [35] LEE, C.—LEE, C.—KIM, C. S.: Contrast Enhancement Based on Layered Difference Representation of 2D Histograms. *IEEE Transactions on Image Processing*, Vol. 22, 2013, No. 12, pp. 5372–5384, doi: 10.1109/TIP.2013.2284059.
- [36] CELIK, T.—TJAHJADI, T.: Contextual and Variational Contrast Enhancement. *IEEE Transactions on Image Processing*, Vol. 20, 2011, No. 12, pp. 3431–3441, doi: 10.1109/TIP.2011.2157513.

- [37] ADELSON, E.—ANDERSON, C.—BERGEN, J.—BURT, P.—OGDEN, J.: Pyramid Methods in Image Processing. *RCA Engineer*, Vol. 29, 1984, No. 6, pp. 33–41.
- [38] YANG, W.—WANG, S.—FANG, Y.—WANG, Y.—LIU, J.: From Fidelity to Perceptual Quality: A Semi-Supervised Approach for Low-Light Image Enhancement. 2020 IEEE/CVF Conference on Computer Vision and Pattern Recognition (CVPR), 2020, pp. 3060–3069, doi: 10.1109/CVPR42600.2020.00313.
- [39] XIAO, C.—SHI, Z.: Adaptive Bilateral Filtering and Its Application in Retinex Image Enhancement. 2013 Seventh International Conference on Image and Graphics (ICIG), 2013, pp. 45–49, doi: 10.1109/ICIG.2013.15.
- [40] XU, L.—YAN, Q.—XIA, Y.—JIA, J.: Structure Extraction from Texture via Relative Total Variation. *ACM Transactions on Graphics*, Vol. 31, 2012, No. 6, Art. No. 139, doi: 10.1145/2366145.2366158.
- [41] REN, X.—YANG, W.—CHENG, W. H.—LIU, J.: LR3M: Robust Low-Light Enhancement via Low-Rank Regularized Retinex Model. *IEEE Transactions on Image Processing*, Vol. 29, 2020, pp. 5862–5876, doi: 10.1109/TIP.2020.2984098.
- [42] LV, F.—LU, F.—WU, J.—LIM, C.: MBLLEN: Low-Light Image/Video Enhancement Using CNNs. *British Machine Vision Conference 2018*, 2018, <https://bmva-archive.org.uk/bmvc/2018/contents/papers/0700.pdf>.
- [43] ZHAO, Z.—XIONG, B.—WANG, L.—OU, Q.—YU, L.—KUANG, F.: RetinexDIP: A Unified Deep Framework for Low-Light Image Enhancement. *IEEE Transactions on Circuits and Systems for Video Technology*, Vol. 32, 2022, No. 3, pp. 1076–1088, doi: 10.1109/TCSVT.2021.3073371.
- [44] WU, W.—WENG, J.—ZHANG, P.—WANG, X.—YANG, W.—JIANG, J.: URetinex-Net: Retinex-Based Deep Unfolding Network for Low-Light Image Enhancement. 2022 IEEE/CVF Conference on Computer Vision and Pattern Recognition (CVPR), 2022, pp. 5891–5900, doi: 10.1109/CVPR52688.2022.00581.
- [45] LI, C.—GUO, C.—LOY, C. C.: Learning to Enhance Low-Light Image via Zero-Reference Deep Curve Estimation. *IEEE Transactions on Pattern Analysis and Machine Intelligence*, Vol. 44, 2022, No. 8, pp. 4225–4238, doi: 10.1109/TPAMI.2021.3063604.
- [46] NI, Z.—YANG, W.—WANG, H.—WANG, S.—MA, L.—KWONG, S.: Cycle-Interactive Generative Adversarial Network for Robust Unsupervised Low-Light Enhancement. *Proceedings of the 30th ACM International Conference on Multimedia (MM '22)*, 2022, pp. 1484–1492, doi: 10.1145/3503161.3548006.
- [47] FU, X.—LIAO, Y.—ZENG, D.—HUANG, Y.—ZHANG, X. P.—DING, X.: A Probabilistic Method for Image Enhancement with Simultaneous Illumination and Reflectance Estimation. *IEEE Transactions on Image Processing*, Vol. 24, 2015, No. 12, pp. 4965–4977, doi: 10.1109/TIP.2015.2474701.
- [48] HE, R.—GUAN, M.—WEN, C.: SCENS: Simultaneous Contrast Enhancement and Noise Suppression for Low-Light Images. *IEEE Transactions on Industrial Electronics*, Vol. 68, 2021, No. 9, pp. 8687–8697, doi: 10.1109/TIE.2020.3013783.
- [49] TSENG, P.: Convergence of a Block Coordinate Descent Method for Nondifferentiable Minimization. *Journal of Optimization Theory and Applications*, Vol. 109, 2001, No. 3, pp. 475–494, doi: 10.1023/A:1017501703105.

- [50] CANDÈS, E. J.—WAKIN, M. B.—BOYD, S. P.: Enhancing Sparsity by Reweighted ℓ_1 Minimization. *Journal of Fourier Analysis and Applications*, Vol. 14, 2008, No. 5-6, pp. 877–905, doi: 10.1007/s00041-008-9045-x.
- [51] BARRETT, R.—BERRY, M.—CHAN, T. F.—DEMME, J.—DONATO, J.—DONGARRA, J.—ELJKHOUT, V.—POZO, R.—ROMINE, C.—VAN DER VORST, H.: *Templates for the Solution of Linear Systems: Building Blocks for Iterative Methods*. Society for Industrial and Applied Mathematics (SIAM), 1994, doi: 10.1137/1.9781611971538.
- [52] MITTAL, A.—SOUNDARARAJAN, R.—BOVIK, A. C.: Making a “Completely Blind” Image Quality Analyzer. *IEEE Signal Processing Letters*, Vol. 20, 2013, No. 3, pp. 209–212, doi: 10.1109/LSP.2012.2227726.
- [53] SINGH, N.—BHANDARI, A. K.: Principal Component Analysis-Based Low-Light Image Enhancement Using Reflection Model. *IEEE Transactions on Instrumentation and Measurement*, Vol. 70, 2021, pp. 1–10, doi: 10.1109/TIM.2021.3096266.
- [54] FU, Z.—YANG, Y.—TU, X.—HUANG, Y.—DING, X.—MA, K. K.: Learning a Simple Low-Light Image Enhancer from Paired Low-Light Instances. 2023 IEEE/CVF Conference on Computer Vision and Pattern Recognition (CVPR), 2023, pp. 22252–22261, doi: 10.1109/CVPR52729.2023.02131.
- [55] WANG, Q.—FU, X.—ZHANG, X. P.—DING, X.: A Fusion-Based Method for Single Backlit Image Enhancement. 2016 IEEE International Conference on Image Processing (ICIP), 2016, pp. 4077–4081, doi: 10.1109/ICIP.2016.7533126.
- [56] MA, K.—ZENG, K.—WANG, Z.: Perceptual Quality Assessment for Multi-Exposure Image Fusion. *IEEE Transactions on Image Processing*, Vol. 24, 2015, No. 11, pp. 3345–3356, doi: 10.1109/TIP.2015.2442920.
- [57] WANG, S.—ZHENG, J.—HU, H. M.—LI, B.: Naturalness Preserved Enhancement Algorithm for Non-Uniform Illumination Images. *IEEE Transactions on Image Processing*, Vol. 22, 2013, No. 9, pp. 3538–3548, doi: 10.1109/TIP.2013.2261309.
- [58] CAI, J.—GU, S.—ZHANG, L.: Learning a Deep Single Image Contrast Enhancer from Multi-Exposure Images. *IEEE Transactions on Image Processing*, Vol. 27, 2018, No. 4, pp. 2049–2062, doi: 10.1109/TIP.2018.2794218.
- [59] ZHANG, L.—ZHANG, L.—MOU, X.—ZHANG, D.: FSIM: A Feature Similarity Index for Image Quality Assessment. *IEEE Transactions on Image Processing*, Vol. 20, 2011, No. 8, pp. 2378–2386, doi: 10.1109/TIP.2011.2109730.
- [60] GU, K.—WANG, S.—ZHAI, G.—MA, S.—YANG, X.—LIN, W.—ZHANG, W.—GAO, W.: Blind Quality Assessment of Tone-Mapped Images via Analysis of Information, Naturalness, and Structure. *IEEE Transactions on Multimedia*, Vol. 18, 2016, No. 3, pp. 432–443, doi: 10.1109/TMM.2016.2518868.



Jun Li received his Ph.D. degree from the University of Munich, Germany. He is currently the Director of the Fujian Robotics Intelligent System Engineering Technology Research Center. He was a Post-Doctoral Research Associate with the University of Marburg, Germany. In 2015, he joined the faculty with the Haixi Institute, Chinese Academy of Sciences. His research focuses on image processing and recognition, robot adaptive control, and human-computer interaction. In the field of images and robots, he has published two personal English and German monograph, published more than 40 innovative academic papers in IEEE

and other SCI journals, applied more than 30 invention patents, and obtained three national invention patents. In 2016, he was selected as a member of the Fujian Provincial Double-Hundred-Talent Program. Since 2015, he has been the Leader of the Laboratory of Robotics and Intelligent Systems hosted and participated different scientific research programs, including the national 13th Five-Year Key Research Program and Fujian Major Science and Technology projects.



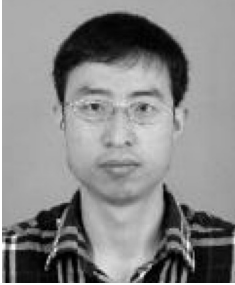
Chao Yan received his B.Sc. degree in computer science and technology from the Henan Polytechnic University in 2017. He is currently pursuing his Master's degree in software engineering at the Fujian Normal University while studying at the Quanzhou Institute of Equipment Manufacturing, Chinese Academy of Sciences. His research interests include computer vision and image enhancement.



Qinglu Hou graduated from the Shandong Agricultural University in 2017, majoring in mathematics and applied mathematics, with the Bachelor of Science degree. He is currently studying for his Master's degree in applied statistics at the Lanzhou Jiaotong University, and at the same time studying at the Quanzhou Institute of Equipment Manufacturing, Chinese Academy of Sciences. His research interests include computer vision and motion deblurring.



Weiwei ZHOU received her B.Sc. degree in applied statistics from the Anhui Agricultural University in 2021. She is currently pursuing a Master's degree in applied statistics at the Lanzhou Jiaotong University and is a guest graduate student at the Quanzhou Equipment Manufacturing, Chinese Academy of Sciences. Her research interests include computer vision and image smoothing.



Yin GAO received his M.Sc. degree in optical engineering from the Yunnan Normal University, China, in 2012. From 2012 to 2020, he was a Senior Engineer with the Image Processing, Quanzhou Institute of Equipment Manufacturing, CAS, Quanzhou, China. He has published more than 20 innovative academic papers in Elsevier and other SCI journals. He is currently a doctoral student at the University of the Chinese Academy of Sciences, and his research interests include image dehazing, low-light image enhancement, multi-exposure image fusion, fundamental study of image optimization, and product identification and defect detection in industrial applications.